Complex variable element-free Galerkin method for viscoelasticity problems*

Cheng Yu-Min(程玉民)[a)†], Li Rong-Xin(李荣鑫)[b)], and Peng Miao-Juan(彭妙娟)[b)]

[a)] *Shanghai Institute of Applied Mathematics and Mechanics, Shanghai University, Shanghai* 200072, *China*
[b)] *Department of Civil Engineering, Shanghai University, Shanghai* 200072, *China*

(Received 6 April 2012; revised manuscript received 18 April 2012)

Based on the complex variable moving least-square (CVMLS) approximation, the complex variable element-free Galerkin (CVEFG) method for two-dimensional viscoelasticity problems under the creep condition is presented in this paper. The Galerkin weak form is employed to obtain the equation system, and the penalty method is used to apply the essential boundary conditions, then the corresponding formulae of the CVEFG method for two-dimensional viscoelasticity problems under the creep condition are obtained. Compared with the element-free Galerkin (EFG) method, with the same node distribution, the CVEFG method has a higher precision, and to obtain the similar precision, the CVEFG method has a greater computational efficiency. Some numerical examples are given to demonstrate the validity and the efficiency of the method in this paper.

Keywords: meshless method, complex variable moving least-square approximation, complex variable element-free Galerkin method, viscoelasticity

PACS: 02.60.Cb, 02.60.Lj, 46.35.+z **DOI:** 10.1088/1674-1056/21/9/090205

1. Introduction

The meshless method has shown some advantages over the traditional numerical methods, such as the finite element method (FEM) and the boundary element method (BEM), and has been successfully developed and applied to a variety of engineering problems.[1−13]

The moving least-square (MLS) approximation is an important method to form the shape function in the meshless method.[14] However, the MLS approximation is the approximation of a scalar function, thus the meshless methods derived from it require a lot of nodes in the domain, and more CPU time is spent compared with the FEM and the BEM.[15,16]

The complex variable moving least-square (CVMLS) approximation, which is an approximation of a vector function, has been developed.[15,16] In the CVMLS approximation, the trial function of a two-dimensional (2D) problem is formed with a one-dimensional (1D) basis function. The number of unknown coefficients in the trial function of the CVMLS approximation is less than that of the MLS approximation. Therefore, without loss of precision, fewer nodes are required to be selected in the meshless method formed from the CVMLS approximation compared to that required in the meshless method with the MLS approximation. Then under the same numerical precision, the meshless method derived from the CVMLS approximation has greater computational efficiency than the one based on the MLS approximation, and the meshless method based on the CVMLS approximation will has a higher precision for the same node distribution.

Based on the CVMLS approximation, the meshless method with complex variable for elasticity problem,[17] the complex variable boundary element-free method for two-dimensional elasticity and elastodynamics problems,[18,19] the complex variable reproducing kernel partical method for two-dimensional elastoplasticity and elastodynamics problems,[20,21] and the complex variable element-free Galerkin (CVEFG) method for two-dimensional elasticity, elastoplasticity, and large deformation problems have been presented.[22−24] Based on an improved CVMLS approximation, an improved complex variable element-free Galerkin method has been developed to solve the two-dimensional elasticity problem.[25]

*Project supported by the National Natural Science Foundation of China (Grant No. 11171208) and the Shanghai Leading Academic Discipline Project, China (Grant No. S30106).

†Corresponding author. E-mail: ymcheng@shu.edu.cn

© 2012 Chinese Physical Society and IOP Publishing Ltd

Viscoelasticity is important in mechanics and engineering. Yang and Liu studied two-dimensional viscoelasticity problems by using a combined approach of element-free Galerkin method and precise algorithm in time domain.[26] Using the MLPG method, anisotropic and linear viscoelastic solids were analyzed by Sladek *et al.*, and quasistatic and transient dynamic problems in two-dimensional linear viscoelastic media were discussed.[27,28] Guan *et al.* discussed the massive metal forming process based on the rigid/viscoplastic element-free Galerkin method.[29] A boundary knot method for harmonic elastic and viscoelastic problems was discussed by Canelas and Sensale.[30]

Based on the CVMLS approximation, the CVEFG method for two-dimensional viscoelasticity problems under the creep condition are presented in this paper. The Galerkin weak form is employed to obtain the equation system, and the penalty method is used to apply the essential boundary conditions, then the corresponding formulae of the CVEFG method for two-dimensional viscoelasticity problems under the creep condition are obtained. Some numerical examples are given to demonstrate the validity and the efficiency of the method in this paper.

2. Complex variable moving least-square approximation

In the CVMLS approximation, the trial function is

$$\begin{aligned}\bar{u}^{\rm h}(z) &= u_1^{\rm h}(z) + {\rm i}u_2^{\rm h}(z) = \sum_{i=1}^{m} p_i(z)\cdot a_i(z)\\ &= \boldsymbol{p}^{\rm T}(z)\cdot\boldsymbol{a}(z), \quad (z = x_1 + {\rm i}x_2 \in \Omega), \end{aligned} \tag{1}$$

where $\bar{u}^{\rm h}(z)$ is the approximation to function $u(z)$, $\boldsymbol{p}^{\rm T}(z) = (p_1(z), p_2(z), \ldots, p_m(z))$ is the basis function vector, $\boldsymbol{a}^{\rm T}(z) = (a_1(z), a_2(z), \ldots, a_m(z))$ is the corresponding coefficient vector, and m is the number of terms in the basis function vector.

In general, the linear and the quadratic basis function vectors in 2D are given respectively by

$$\boldsymbol{p}^{\rm T} = (1, z), \tag{2}$$

$$\boldsymbol{p}^{\rm T} = (1, z, z^2). \tag{3}$$

The local approximation at point z is defined by

$$\bar{u}^{\rm h}(z, \bar{z}) = \sum_{i=1}^{m} p_i(\bar{z})\cdot a_i(z) = \boldsymbol{p}^{\rm T}(\bar{z})\cdot\boldsymbol{a}(z), \tag{4}$$

where $\bar{z}$ is the point in the local domain of z.

Define

$$\begin{aligned} J &= \sum_{I=1}^{n} w(z - z_I)[\bar{u}^{\rm h}(z, z_I) - \bar{u}(z_I)]^2\\ &= (\boldsymbol{P}\boldsymbol{a} - \bar{\boldsymbol{u}})^{\rm T}\boldsymbol{W}(z)(\boldsymbol{P}\boldsymbol{a} - \bar{\boldsymbol{u}}), \end{aligned} \tag{5}$$

where $w(z - z_I)$ is a weight function with compact support, z_I $(I = 1, 2, \ldots, n)$ are the nodes with domains of influence that cover point z, and

$$\bar{u}(z_I) = u_1(z_I) + {\rm i}u_2(z_I), \tag{6}$$

$$\bar{\boldsymbol{u}} = (\bar{u}(z_1), \bar{u}(z_2), \ldots, \bar{u}(z_n))^{\rm T} = \boldsymbol{Q}\boldsymbol{u}, \tag{7}$$

$$\begin{aligned}\boldsymbol{u} = (&u_1(z_1), u_2(z_1), u_1(z_2), u_2(z_2), \ldots,\\ &u_1(z_n), u_2(z_n))^{\rm T}, \end{aligned} \tag{8}$$

$$\boldsymbol{Q} = \begin{bmatrix} 1 & {\rm i} & 0 & 0 & 0 & 0 & \ldots & 0 & 0\\ 0 & 0 & 1 & {\rm i} & 0 & 0 & \ldots & 0 & 0\\ 0 & 0 & 0 & 0 & 1 & {\rm i} & \ldots & 0 & 0\\ \vdots & \vdots & \vdots & \vdots & \vdots & \vdots & \ddots & \vdots & \vdots\\ 0 & 0 & 0 & 0 & 0 & 0 & \ldots & 1 & {\rm i} \end{bmatrix}_{n\times 2n}, \tag{9}$$

$$\boldsymbol{P} = \begin{bmatrix} p_1(z_1) & p_2(z_1) & \ldots & p_m(z_1)\\ p_1(z_2) & p_2(z_2) & \ldots & p_m(z_2)\\ \vdots & \vdots & \ddots & \vdots\\ p_1(z_n) & p_2(z_n) & \ldots & p_m(z_n) \end{bmatrix}, \tag{10}$$

$$\boldsymbol{W}(z) = \begin{bmatrix} w(z - z_1) & 0 & \ldots & 0\\ 0 & w(z - z_2) & \ldots & 0\\ \vdots & \vdots & \ddots & \vdots\\ 0 & 0 & \ldots & w(z - z_n) \end{bmatrix}. \tag{11}$$

From $\partial J/\partial \boldsymbol{a} = 0$, we have

$$\boldsymbol{A}(z)\boldsymbol{a}(z) = \boldsymbol{B}(z)\bar{\boldsymbol{u}}, \tag{12}$$

where

$$\boldsymbol{A}(z) = \boldsymbol{P}^{\rm T}\boldsymbol{W}(z)\boldsymbol{P}, \tag{13}$$

$$\boldsymbol{B}(z) = \boldsymbol{P}^{\rm T}\boldsymbol{W}(z), \tag{14}$$

then

$$\boldsymbol{a}(z) = \boldsymbol{A}^{-1}(z)\boldsymbol{B}(z)\bar{\boldsymbol{u}}. \tag{15}$$

The expression for the local approximation $\bar{u}^{\rm h}(z)$ is

$$\bar{u}^{\rm h}(z) = \bar{\boldsymbol{\Phi}}(z)\bar{\boldsymbol{u}} = \sum_{I=1}^{n} \bar{\Phi}_I(z)\bar{u}(z_I), \tag{16}$$

where $\bar{\boldsymbol{\Phi}}(z)$ is called the shape function, and

$$\bar{\boldsymbol{\Phi}}(z) = (\bar{\Phi}_1(z), \bar{\Phi}_2(z), \ldots, \bar{\Phi}_n(z))$$

$$= \boldsymbol{p}^{\mathrm{T}}(z)\boldsymbol{A}^{-1}(z)\boldsymbol{B}(z), \tag{17}$$

From Eq. (16) we have

$$u_1^{\mathrm{h}}(z) = \mathrm{Re}[\bar{\boldsymbol{\Phi}}(z)\bar{\boldsymbol{u}}] = \mathrm{Re}\left[\sum_{I=1}^{n}\bar{\Phi}_I(z)\bar{u}(z_I)\right], \tag{18}$$

$$u_2^{\mathrm{h}}(z) = \mathrm{Im}[\bar{\boldsymbol{\Phi}}(z)\bar{\boldsymbol{u}}] = \mathrm{Im}\left[\sum_{I=1}^{n}\bar{\Phi}_I(z)\bar{u}(z_I)\right]. \tag{19}$$

As shown in Eq. (1), in the CVMLS approximation, the trial function of a two-dimensional problem is formed with a one-dimensional basis function. Then the number of unknown coefficients in the trial function of the CVMLS approximation is less than that in the trial function of the MLS approximation. In the MLS approximation, the linear basis is $\boldsymbol{p}^{\mathrm{T}} = (1, x_1, x_2)$, and three unknown coefficients are included in the trial function, whereas in the CVMLS approximation, the linear basis is $\boldsymbol{p}^{\mathrm{T}} = (1, z)$, and two unknown coefficients are included in the trial function. In the MLS approximation, the quadratic basis is $\boldsymbol{p}^{\mathrm{T}} = (1, x_1, x_2, x_1^2, x_1x_2, x_2^2)$, and six unknown coefficients are included in the trial function, whereas in the CVMLS approximation, the quadratic basis is $\boldsymbol{p}^{\mathrm{T}} = (1, z, z^2)$, and three unknown coefficients are included in the trial function. For an arbitrary point in the domain, we need fewer nodes with domains of influence that cover the point, and thus we also require fewer nodes in the whole domain. Under the same numerical precision, the meshless method derived from the CVMLS approximation has a greater computational efficiency. If we select the same nodes in the whole domain, then the meshless method derived from the CVMLS approximation has higher computational precision than that derived from the MLS approximation.

In addition, because the number of unknown coefficients in the CVMLS approximation is less than that in the MLS approximation, the order of Eq. (12) in the CVMLS approximation is less than that in the MLS approximation. Then equation (12) can be solved more easily, and less CPU time is required. Because we require fewer nodes in the whole domain in the CVMLS approximation, fewer shape functions are obtained, and the CPU time will be decreased further.

3. The CVEFG method for two-dimensional viscoelasticity problems

3.1. Constitutive relationships of viscoelasticity

The Maxwell model and the Kelvin model are two typical constitutive models of viscoelastic materials.[31] When linear viscoelastic materials are located by a constant stress $\sigma = \sigma_0 H(t)$, where $H(t)$ is the Heaviside unit step function, the strain is time dependent, and

$$\varepsilon(t) = \sigma_0 J(t), \tag{20}$$

where $J(t)$ is the creep function.

The creep function of the Maxwell model is

$$J(t) = \frac{1}{G} + \frac{t}{\eta}, \tag{21}$$

the one of the Kelvin model is

$$J(t) = \frac{1}{G}(1 - \mathrm{e}^{-Gt/\eta}), \tag{22}$$

and the one of the three-parameter model is

$$J(t) = \frac{1}{G_2} + \frac{1}{G_1}(1 - \mathrm{e}^{-G_1 t/\eta}), \tag{23}$$

where G, G_1, and G_2 are the shear elastic moduli, and η is the viscosity constant of each model.

In the case of small deformation, the stress tensor $\boldsymbol{\sigma}$ can be decomposed into the spherical tensor and the deviatoric tensor, i.e.,

$$\boldsymbol{\sigma} = \begin{bmatrix} \sigma_{11} & \sigma_{12} & \sigma_{13} \\ \sigma_{21} & \sigma_{22} & \sigma_{23} \\ \sigma_{31} & \sigma_{32} & \sigma_{33} \end{bmatrix} = \begin{bmatrix} \sigma_{\mathrm{v}} & 0 & 0 \\ 0 & \sigma_{\mathrm{v}} & 0 \\ 0 & 0 & \sigma_{\mathrm{v}} \end{bmatrix} + \begin{bmatrix} \sigma_{11} - \sigma_{\mathrm{v}} & \sigma_{12} & \sigma_{13} \\ \sigma_{21} & \sigma_{22} - \sigma_{\mathrm{v}} & \sigma_{23} \\ \sigma_{31} & \sigma_{32} & \sigma_{33} - \sigma_{\mathrm{v}} \end{bmatrix}, \tag{24}$$

where the first term on the right-hand side is the spherical stress tensor, the second term is the deviatoric stress tensor S_{ij}, and

$$\sigma_{\mathrm{v}} = \frac{\sigma_{ii}}{3} = \frac{(\sigma_{11} + \sigma_{22} + \sigma_{33})}{3}. \tag{25}$$

The strain tensor $\boldsymbol{\varepsilon}$ can be similarly decomposed into the volume deformation tensor and the shape distortion tensor, i.e.,

$$\boldsymbol{\varepsilon} = \begin{bmatrix} \varepsilon_{11} & \varepsilon_{12} & \varepsilon_{13} \\ \varepsilon_{21} & \varepsilon_{22} & \varepsilon_{23} \\ \varepsilon_{31} & \varepsilon_{32} & \varepsilon_{33} \end{bmatrix} = \begin{bmatrix} e & 0 & 0 \\ 0 & e & 0 \\ 0 & 0 & e \end{bmatrix}$$

$$+\begin{bmatrix} \varepsilon_{11}-e & \varepsilon_{12} & \varepsilon_{13} \\ \varepsilon_{21} & \varepsilon_{22}-e & \varepsilon_{23} \\ \varepsilon_{31} & \varepsilon_{32} & \varepsilon_{33}-e \end{bmatrix}, \tag{26}$$

where the first term on the right-hand side is the spherical strain tensor, the second term is the deviatoric strain tensor e_{ij}, and

$$e=\frac{\varepsilon_{ii}}{3}=\frac{(\varepsilon_{11}+\varepsilon_{22}+\varepsilon_{33})}{3}. \tag{27}$$

In the three-dimensional case, there are two creep compliances, $J_1(t)$ and $J_2(t)$, which describe the features of deviatoric and spherical parts, respectively. The rheological property is obtained mainly by the shear deformation. Then we assume the volume deformation is elastic as follows.

Under the location $\sigma = \sigma_0 H(t)$, the three-dimensional constitutive relationship of viscoelastic materials can be written as

$$\begin{cases} e_{ij}(t)=J_1(t)S_{ij}, \\ e(t)=J_2(t)\sigma_{\rm v}, \end{cases} \tag{28}$$

where $J_1(t)$ is the creep compliance in Eqs. (22)–(24), and

$$J_2(t)=\frac{1}{3K}, \tag{29}$$

with K being the volumetric modulus of elasticity.

3.2. The CVEFG method for two-dimensional viscoelasticity problems

The stress–strain relationship in linear viscoelasticity problems appears to be time-dependent, thus the material parameters depend on time. Suppose that the stress $\boldsymbol{\sigma}$ is constant throughout the loading process, while the strain $\boldsymbol{\varepsilon}(t)$ and the displacement $\boldsymbol{u}(t)$ vary with time. If the body force $\boldsymbol{b}$ in the solving domain, the traction $\bar{\boldsymbol{t}}$ on the natural boundary Γ_t, and the displacement $\bar{\boldsymbol{u}}$ on the essential boundary Γ_u are given (the boundary conditions are constant), the basic equations and the boundary conditions can be written as follows.

The equilibrium equation is

$$\boldsymbol{L}^{\rm T}\boldsymbol{\sigma}+\boldsymbol{b}=0, \quad (x\in\Omega), \tag{30}$$

where $\boldsymbol{L}$ is the differential operator matrix, i.e.,

$$\boldsymbol{L}=\begin{bmatrix} \dfrac{\partial}{\partial x_1} & 0 \\ 0 & \dfrac{\partial}{\partial x_2} \\ \dfrac{\partial}{\partial x_2} & \dfrac{\partial}{\partial x_1} \end{bmatrix}. \tag{31}$$

The strain–displacement relationship is

$$\boldsymbol{\varepsilon}=\boldsymbol{L}\boldsymbol{u}, \quad (x\in\Omega). \tag{32}$$

The stress–strain relationship is

$$\boldsymbol{\sigma}(z)=\boldsymbol{M}_1\begin{Bmatrix} e \\ e \\ 0 \end{Bmatrix}+\boldsymbol{M}_2\begin{Bmatrix} e_{11} \\ e_{22} \\ e_{12} \end{Bmatrix}, \tag{33}$$

where

$$\boldsymbol{M}_1=\begin{bmatrix} 3K & 0 & 0 \\ 0 & 3K & 0 \\ 0 & 0 & 3K \end{bmatrix}, \tag{34}$$

$$\boldsymbol{M}_2=\begin{bmatrix} \dfrac{1}{J_1(t)} & 0 & 0 \\ 0 & \dfrac{1}{J_1(t)} & 0 \\ 0 & 0 & \dfrac{1}{J_1(t)} \end{bmatrix}. \tag{35}$$

The boundary conditions are

$$\boldsymbol{u}=\bar{\boldsymbol{u}}, \quad (x\in\Gamma_u), \tag{36}$$

$$\boldsymbol{n}\cdot\boldsymbol{\sigma}=\bar{t}, \quad (x\in\Gamma_t), \tag{37}$$

where

$$\boldsymbol{n}=\begin{bmatrix} n_1 & 0 & n_2 \\ 0 & n_2 & n_1 \end{bmatrix}, \tag{38}$$

and n_1 and n_2 are the units outward normal to boundary Γ_t, respectively.

From the CVMLS approximation (16), the displacement $\bar{\boldsymbol{u}}(z)$ at an arbitrary point z in the domain can be expressed as

$$\begin{aligned} \bar{u}(z) &= u_1(z)+{\rm i}u_2(z)=\bar{\boldsymbol{\Phi}}(z)\bar{\boldsymbol{u}} \\ &= \sum_{I=1}^{n}\bar{\Phi}_I(z)\bar{u}(z_I), \end{aligned} \tag{39}$$

where $\bar{\boldsymbol{\Phi}}(z)$ is the vector of the shape function, and

$$\bar{u}(z_I)=u_1(z_I)+{\rm i}u_2(z_I). \tag{40}$$

Combining Eq. (39) with Eq. (40), we have

$$\boldsymbol{u}(z)=\left\{\begin{array}{c}u_1(z)\\u_2(z)\end{array}\right\}=\sum_I^n\left[\begin{array}{cc}\mathrm{Re}[\bar{\Phi}_I(z)] & -\mathrm{Im}[\bar{\Phi}_I(z)]\\ \mathrm{Im}[\bar{\Phi}_I(z)] & \mathrm{Re}[\bar{\Phi}_I(z)]\end{array}\right]\cdot\left\{\begin{array}{c}u_1(z_I)\\u_2(z_I)\end{array}\right\}=\sum_I^n\tilde{\boldsymbol{\Phi}}_I(z)\cdot\boldsymbol{u}_I=\tilde{\boldsymbol{\Phi}}(z)\cdot\boldsymbol{U},\tag{41}$$

where $\tilde{\boldsymbol{\Phi}}(z)$ is the matrix of shape functions, n is the number of nodes in the support domain of point z, and $\boldsymbol{U}$ is the nodal displacement vector

$$\tilde{\boldsymbol{\Phi}}(z)=(\tilde{\boldsymbol{\Phi}}_1(z),\tilde{\boldsymbol{\Phi}}_2(z),\ldots,\tilde{\boldsymbol{\Phi}}_n(z)),\tag{42}$$

$$\tilde{\boldsymbol{\Phi}}_I(z)=\left[\begin{array}{cc}\mathrm{Re}[\bar{\Phi}_I(z)] & -\mathrm{Im}[\bar{\Phi}_I(z)]\\ \mathrm{Im}[\bar{\Phi}_I(z)] & \mathrm{Re}[\bar{\Phi}_I(z)]\end{array}\right],\tag{43}$$

$$\boldsymbol{U}^{\mathrm{T}}=(\boldsymbol{u}^{\mathrm{T}}(z_1),\boldsymbol{u}^{\mathrm{T}}(z_2),\ldots,\boldsymbol{u}^{\mathrm{T}}(z_n)),\tag{44}$$

$$\boldsymbol{u}(z_I)=\left\{\begin{array}{c}u_1(z_I)\\u_2(z_I)\end{array}\right\}.\tag{45}$$

The strain tensor of two-dimensional viscoelastisity problems can be written as

$$\begin{aligned}\boldsymbol{\varepsilon}(z)&=\left\{\begin{array}{c}\varepsilon_{11}(z)\\\varepsilon_{22}(z)\\\varepsilon_{12}(z)\end{array}\right\}=\boldsymbol{L}\bar{\boldsymbol{u}}(z)=\boldsymbol{L}(\tilde{\boldsymbol{\Phi}}(z)\bar{\boldsymbol{u}})=\boldsymbol{L}(\tilde{\boldsymbol{\Phi}}(z)\boldsymbol{Q}\boldsymbol{u})\\&=\left[\begin{array}{c}(\mathrm{Re}[\sum\limits_{I=1}^n\bar{\Phi}_I(z)\bar{u}(z_I)])_{,1}\\(\mathrm{Im}[\sum\limits_{I=1}^n\bar{\Phi}_I(z)\bar{u}(z_I)])_{,2}\\(\mathrm{Re}[\sum\limits_{I=1}^n\bar{\Phi}_I(z)\bar{u}(z_I)])_{,2}+(\mathrm{Im}[\sum\limits_{I=1}^n\bar{\Phi}_I(z)\bar{u}(z_I)])_{,1}\end{array}\right]=\boldsymbol{B}(z)\cdot\boldsymbol{u},\end{aligned}\tag{46}$$

where

$$\boldsymbol{B}(z)=(\boldsymbol{B}_1(z),\boldsymbol{B}_2(z),\ldots,\boldsymbol{B}_n(z)),\tag{47}$$

$$\boldsymbol{B}_I(z)=\left[\begin{array}{cc}\mathrm{Re}[\bar{\Phi}_{I,1}(z)] & -\mathrm{Im}[\bar{\Phi}_{I,1}(z)]\\ \mathrm{Im}[\bar{\Phi}_{I,2}(z)] & \mathrm{Re}[\bar{\Phi}_{I,2}(z)]\\ \mathrm{Re}[\bar{\Phi}_{I,2}(z)]+\mathrm{Im}[\bar{\Phi}_{I,1}(z)] & -\mathrm{Im}[\bar{\Phi}_{I,2}(z)]+\mathrm{Re}[\bar{\Phi}_{I,1}(z)]\end{array}\right],\tag{48}$$

$$\boldsymbol{u}=(u_1(z_1),u_2(z_1),u_1(z_2),u_2(z_2),\ldots,u_1(z_n),u_2(z_n))^{\mathrm{T}}.\tag{49}$$

The stress tensor of two-dimensional viscoelastisity problems can be written as

$$\begin{aligned}\boldsymbol{\sigma}(z)&=\left\{\begin{array}{c}\sigma_{11}\\\sigma_{22}\\\sigma_{12}\end{array}\right\}=\left\{\begin{array}{c}\sigma_{\mathrm{v}}\\\sigma_{\mathrm{v}}\\0\end{array}\right\}+\left\{\begin{array}{c}\sigma_{11}-\sigma_{\mathrm{v}}\\\sigma_{22}-\sigma_{\mathrm{v}}\\\sigma_{12}\end{array}\right\}\\&=\boldsymbol{M}_1\left\{\begin{array}{c}e\\e\\0\end{array}\right\}+\boldsymbol{M}_2\left\{\begin{array}{c}e_{11}\\e_{22}\\e_{12}\end{array}\right\},\end{aligned}\tag{50}$$

where

$$\left\{\begin{array}{c}e\\e\\0\end{array}\right\}=\frac{1}{3}\left\{\begin{array}{c}\varepsilon_{11}+\varepsilon_{22}+\varepsilon_{33}\\\varepsilon_{11}+\varepsilon_{22}+\varepsilon_{33}\\0\end{array}\right\}=\boldsymbol{B}^{(1)}(z)\cdot\boldsymbol{u},\tag{51}$$

$$\begin{aligned}\left\{\begin{array}{c}e_{11}\\e_{22}\\e_{12}\end{array}\right\}&=\left\{\begin{array}{c}\varepsilon_{11}-\frac{1}{3}(\varepsilon_{11}+\varepsilon_{22}+\varepsilon_{33})\\\varepsilon_{22}-\frac{1}{3}(\varepsilon_{11}+\varepsilon_{22}+\varepsilon_{33})\\\frac{1}{2}\varepsilon_{12}\end{array}\right\}\\&=\boldsymbol{B}^{(2)}(z)\cdot\boldsymbol{u},\end{aligned}\tag{52}$$

$\boldsymbol{B}^{(1)}(z)$ is the positive strain matrix

$$\boldsymbol{B}^{(1)}(z)=(\boldsymbol{B}_1^{(1)}(z),\boldsymbol{B}_2^{(1)}(z),\ldots,\boldsymbol{B}_n^{(1)}(z)),\tag{53}$$

and $\boldsymbol{B}^{(2)}(z)$ is the deviator strain matrix

$$\boldsymbol{B}^{(2)}(z)=(\boldsymbol{B}_1^{(2)}(z),\boldsymbol{B}_2^{(2)}(z),\ldots,\boldsymbol{B}_n^{(2)}(z)).\tag{54}$$

For the case of plane stress, $\sigma_{33}=0$, and we have

$$\boldsymbol{B}_I^{(1)}(z)=\frac{1}{3KJ_1(t)+2}\cdot\begin{bmatrix}\mathrm{Re}[\bar{\Phi}_{I,1}(z)]+\mathrm{Im}[\bar{\Phi}_{I,2}(z)] & -\mathrm{Im}[\bar{\Phi}_{I,1}(z)]+\mathrm{Re}[\bar{\Phi}_{I,2}(z)]\\ \mathrm{Re}[\bar{\Phi}_{I,1}(z)]+\mathrm{Im}[\bar{\Phi}_{I,2}(z)] & -\mathrm{Im}[\bar{\Phi}_{I,1}(z)]+\mathrm{Re}[\bar{\Phi}_{I,2}(z)]\\ 0 & 0\end{bmatrix}, \tag{55}$$

$$\boldsymbol{B}_I^{(2)}(z)=\begin{bmatrix}\beta_1\mathrm{Re}[\bar{\Phi}_{I,1}(z)]-\beta_2\mathrm{Im}[\bar{\Phi}_{I,2}(z)] & -\beta_1\mathrm{Im}[\bar{\Phi}_{I,1}(z)]-\beta_2\mathrm{Re}[\bar{\Phi}_{I,2}(z)]\\ -\beta_2\mathrm{Re}[\bar{\Phi}_{I,1}(z)]+\beta_1\mathrm{Im}[\bar{\Phi}_{I,2}(z)] & \beta_2\mathrm{Im}[\bar{\Phi}_{I,1}(z)]+\beta_1\mathrm{Re}[\bar{\Phi}_{I,2}(z)]\\ \frac{1}{2}(\mathrm{Re}[\bar{\Phi}_{I,2}(z)]+\mathrm{Im}[\bar{\Phi}_{I,1}(z)]) & \frac{1}{2}(-\mathrm{Im}[\bar{\Phi}_{I,2}(z)]+\mathrm{Re}[\bar{\Phi}_{I,1}(z)])\end{bmatrix}, \tag{56}$$

where β_1 and β_2 are constants, and

$$\beta_1=\frac{3KJ_1(t)+1}{3KJ_1(t)+2}, \tag{57}$$

$$\beta_2=\frac{1}{3KJ_1(t)+2}. \tag{58}$$

For the case of plane strain, $\varepsilon_{33}=0$, we have

$$\boldsymbol{B}_I^{(1)}(z)=\frac{1}{3}\cdot\begin{bmatrix}\mathrm{Re}[\bar{\Phi}_{I,1}(z)]+\mathrm{Im}[\bar{\Phi}_{I,2}(z)] & -\mathrm{Im}[\bar{\Phi}_{I,1}(z)]+\mathrm{Re}[\bar{\Phi}_{I,2}(z)]\\ \mathrm{Re}[\bar{\Phi}_{I,1}(z)]+\mathrm{Im}[\bar{\Phi}_{I,2}(z)] & -\mathrm{Im}[\bar{\Phi}_{I,1}(z)]+\mathrm{Re}[\bar{\Phi}_{I,2}(z)]\\ 0 & 0\end{bmatrix}, \tag{59}$$

$$\boldsymbol{B}_I^{(2)}(z)=\begin{bmatrix}\frac{2}{3}\mathrm{Re}[\bar{\Phi}_{I,1}(z)]-\frac{1}{3}\mathrm{Im}[\bar{\Phi}_{I,2}(z)] & -\frac{2}{3}\mathrm{Im}[\bar{\Phi}_{I,1}(z)]-\frac{1}{3}\mathrm{Re}[\bar{\Phi}_{I,2}(z)]\\ -\frac{2}{3}\mathrm{Re}[\bar{\Phi}_{I,1}(z)]+\frac{1}{3}\mathrm{Im}[\bar{\Phi}_{I,2}(z)] & \frac{2}{3}\mathrm{Im}[\bar{\Phi}_{I,1}(z)]+\frac{1}{3}\mathrm{Re}[\bar{\Phi}_{I,2}(z)]\\ \frac{1}{2}(\mathrm{Re}[\bar{\Phi}_{I,2}(z)]+\mathrm{Im}[\bar{\Phi}_{I,1}(z)]) & \frac{1}{2}(-\mathrm{Im}[\bar{\Phi}_{I,2}(z)]+\mathrm{Re}[\bar{\Phi}_{I,1}(z)])\end{bmatrix}. \tag{60}$$

Substituting Eqs. (51) and (52) into Eq. (50) yields

$$\boldsymbol{\sigma}(z)=\begin{Bmatrix}\sigma_{11}\\ \sigma_{22}\\ \sigma_{12}\end{Bmatrix}=\boldsymbol{M}_1\boldsymbol{B}^{(1)}\boldsymbol{u}+\boldsymbol{M}_2\boldsymbol{B}^{(2)}\boldsymbol{u}. \tag{61}$$

Using the penalty method to apply the essential boundary conditions, the Galerkin weak form of the viscoelasticity problems can be written as

$$\int_\Omega\delta\boldsymbol{\varepsilon}^{\mathrm{T}}\cdot\boldsymbol{\sigma}\,\mathrm{d}\Omega-\int_\Omega\delta\boldsymbol{u}^{\mathrm{T}}\cdot\boldsymbol{b}\mathrm{d}\Omega-\int_{\Gamma_t}\delta\boldsymbol{u}^{\mathrm{T}}\cdot\bar{\boldsymbol{t}}\,\mathrm{d}\,\Gamma_t+\alpha\int_{\Gamma_u}\delta\boldsymbol{u}^{\mathrm{T}}\boldsymbol{S}(\boldsymbol{u}-\bar{\boldsymbol{u}})\,\mathrm{d}\Gamma_u=0. \tag{62}$$

Substituting Eqs. (46) and (61) into Eq. (62) yields

$$\begin{aligned}&\int_\Omega\delta\boldsymbol{U}^{\mathrm{T}}(\boldsymbol{B}^{\mathrm{T}}\cdot\boldsymbol{M}_1\cdot\boldsymbol{B}^{(1)})\boldsymbol{U}\,\mathrm{d}\Omega\\&+\int_\Omega\delta\boldsymbol{U}^{\mathrm{T}}(\boldsymbol{B}^{\mathrm{T}}\cdot\boldsymbol{M}_2\cdot\boldsymbol{B}^{(2)})\boldsymbol{U}\,\mathrm{d}\Omega\\&-\int_\Omega\delta\boldsymbol{U}^{\mathrm{T}}\tilde{\boldsymbol{\Phi}}^{\mathrm{T}}\boldsymbol{b}\mathrm{d}\boldsymbol{\Omega}-\int_{\Gamma_t}\delta\boldsymbol{U}^{\mathrm{T}}\tilde{\boldsymbol{\Phi}}^{\mathrm{T}}\bar{\boldsymbol{t}}\mathrm{d}\,\Gamma_t\\&+\alpha\int_{\Gamma_u}\delta\boldsymbol{U}^{\mathrm{T}}(\tilde{\boldsymbol{\Phi}}^{\mathrm{T}}\cdot\boldsymbol{S}\cdot\tilde{\boldsymbol{\Phi}})\boldsymbol{U}\,\mathrm{d}\,\Gamma_u\\&-\alpha\int_{\Gamma_u}\delta\boldsymbol{U}^{\mathrm{T}}(\tilde{\boldsymbol{\Phi}}^{\mathrm{T}}\cdot\boldsymbol{S}\cdot\bar{u})\mathrm{d}\boldsymbol{\Gamma}_u=0.\end{aligned} \tag{63}$$

Because the variation of the nodal test function $\delta\boldsymbol{U}^{\mathrm{T}}$ is arbitrary, the final discretized equation is obtained as

$$(\boldsymbol{K}+\boldsymbol{K}^\alpha)\cdot\boldsymbol{U}=\boldsymbol{F}+\boldsymbol{F}^\alpha, \tag{64}$$

where

$$\boldsymbol{K}=\int_\Omega\boldsymbol{B}^{\mathrm{T}}\cdot\boldsymbol{M}_1\cdot\boldsymbol{B}^{(1)}\mathrm{d}\,\Omega+\int_\Omega\boldsymbol{B}^{\mathrm{T}}\cdot\boldsymbol{M}_2\cdot\boldsymbol{B}^{(2)}\mathrm{d}\,\Omega, \tag{65}$$

$$\boldsymbol{F}=\int_\Omega\tilde{\boldsymbol{\Phi}}^{\mathrm{T}}(z)\cdot\boldsymbol{b}\mathrm{d}\Omega+\int_{\Gamma_t}\tilde{\boldsymbol{\Phi}}^{\mathrm{T}}(z)\cdot\bar{\boldsymbol{t}}\mathrm{d}\Gamma_t, \tag{66}$$

$$\boldsymbol{K}^\alpha=\alpha\int_{\Gamma_u}\tilde{\boldsymbol{\Phi}}^{\mathrm{T}}(z)\cdot\boldsymbol{S}\cdot\tilde{\boldsymbol{\Phi}}(z)\mathrm{d}\Gamma_u, \tag{67}$$

$$\boldsymbol{F}^\alpha=\alpha\int_{\Gamma_u}\tilde{\boldsymbol{\Phi}}^{\mathrm{T}}(z)\cdot\boldsymbol{S}\cdot\bar{\boldsymbol{u}}\mathrm{d}\Gamma_u, \tag{68}$$

$$\boldsymbol{S}=\begin{bmatrix}s_1 & 0\\ 0 & s_2\end{bmatrix}. \tag{69}$$

When the displacement exists at the boundary along the x_1 (x_2) direction, the corresponding s_1 (s_2) equals to 1, otherwise is 0.

By solving Eq. (64), the nodal displacement vector at any selected time can be obtained. Subsequently, the displacement and the stress of an arbitrary point in the domain can be easily obtained by using Eqs. (41) and (61). And this is the CVEFG method for two-dimensional viscoelasticity problems.

4. Numerical examples

Four examples are presented to demonstrate the applicability of the CVEFG method for two-dimensional viscoelasticity problems. The results obtained using the CVEFG method are compared with the analytical solutions and the ones of the EFG method and the FEM.

In the numerical examples presented in this section, the linear basis function and the cubic spline weight function are used in the CVMLS approximation. The rectangle zone is used as the support domain for a node. In each integration cell, 4×4 Gauss points are used for the Gaussian quadrature, and the distribution of grid points in the background meshes are the same as the node distribution.

4.1. Cantilever beam subjected to a distributed loading

Consider a cantilever beam subjected to a distributed loading, as shown in Fig. 1. The length of the beam is $L = 8$ m, the height is $H = 2$ m, and a unit thickness beam is considered. The distributed loading is $q = 3.0 \times 10^4$ Pa without considering the gravity. The volume deformation is elastic, and $E = 1.0 \times 10^8$ Pa, $\nu = 0.25$. The Kelvin model is adopted to describe the rheological property of the shear deformation, and $G = 2.0 \times 10^8$ Pa, $\eta = 6.0 \times 10^8$ Pa·s. This example is discussed as a plane stress problem.

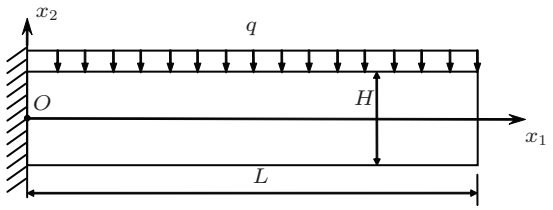


Fig. 1. Cantilever beam subjected to a distributed loading.

As shown in Fig. 2, 13×15 nodes are used in this example. The scaling parameter $d_{\max}$ determining the size of the support domain is 3.7, and the penalty factor is $\alpha = 1.0 \times 10^3 E$.

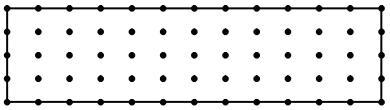


Fig. 2. Node distribution in the cantilever beam.

The numerical results obtained using the CVEFG method are shown in Figs. 3–6 compared with the ones obtained using the EFG method and the FEM with the same node distribution. From Figs. 3–6, we can see that the results obtained using the CVEFG method are in good agreement with the ones obtained using the FEM, and the CVEFG method in this paper has higher precision than the EFG method.

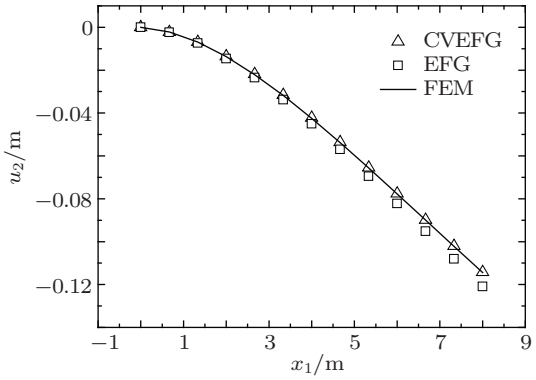


Fig. 3. Vertical displacements of nodes on the neutral axis of the beam when $t = 20$ s.

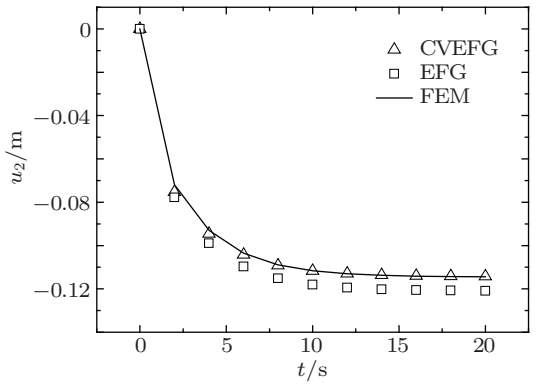


Fig. 4. Time variation of vertical displacement of point (8, 0).

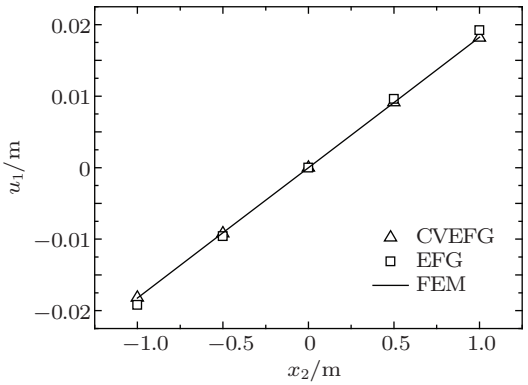


Fig. 5. Horizontal displacements of nodes on the right edge of the beam when $t = 20$ s.

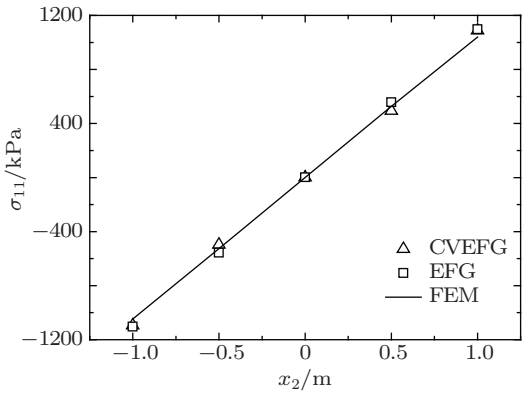


Fig. 6. Horizontal normal stress at $x_1 = 1$ m when $t = 20$ s.

4.2. Beam subjected to a simple bending

A beam subjected to a simple bending is considered, as shown in Fig. 7. The geometric parameters are $L = 5$ m and $H = 2$ m, and a unit thickness beam is considered. The volume deformation is elastic, and $E = 1.0 \times 10^6$ Pa, $\nu = 0.3$. The three-parameter model is adopted to describe the rheological property of the shear deformation, and $G_1 = 5.0 \times 10^5$ Pa, $G_2 = 1.0 \times 10^6$ Pa, $\eta = 2.0 \times 10^6$ P·s. This example is discussed as a plane stress problem without considering the gravity.

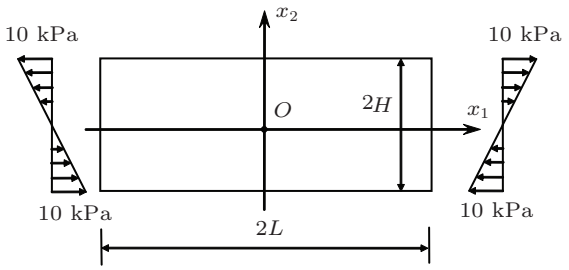


Fig. 7. Beam subjected to a simple bending.

By taking advantage of the symmetry of the model, only a quarter of the model is considered in this analysis. As shown in Fig. 8, 13×7 nodes are used for this example. The scaling parameter $d_{\max}$ is 4.0, and the penalty factor is $\alpha = 1.0 \times 10^2 E$.

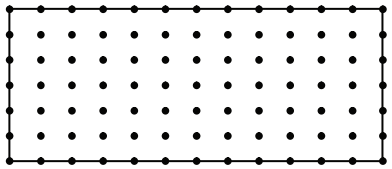


Fig. 8. Node distribution in a quarter of the beam.

Under the same node distribution, the numerical results obtained using the CVEFG method are in good agreement with those obtained uisng the EFG method and the FEM, as shown in Figs. 9–11.

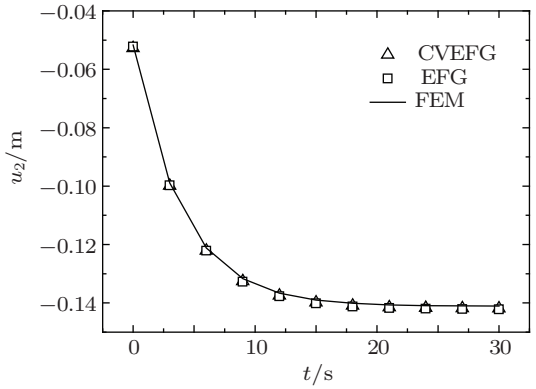


Fig. 9. Time variation of vertical displacement of the midpoint at the right edge of the beam.

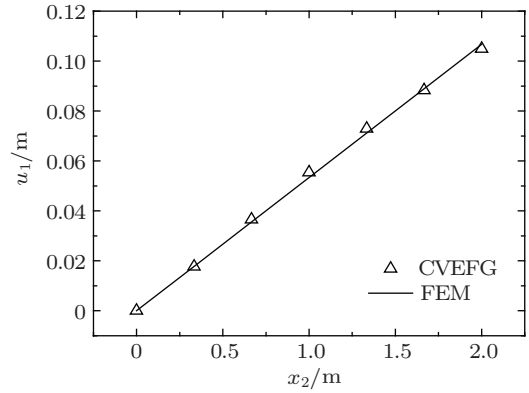


Fig. 10. Horizontal displacements of nodes on the right edge of the beam when $t = 30$ s.

As shown in Fig. 12, to obtain the similar numerical precision, the CPU time used in the CVEFG method is 10.36 s, and that used in the EFG method

is 14.35 s. The CVEFG method has greater computational efficiency than the EFG method.

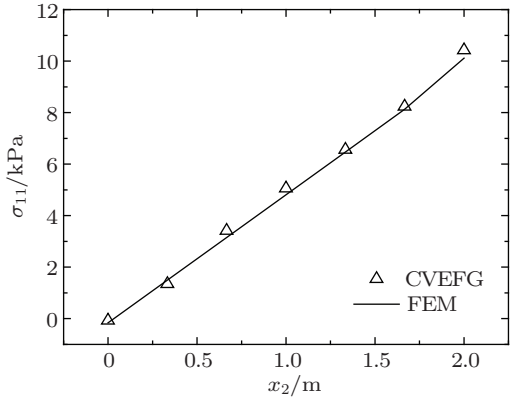


Fig. 11. Horizontal normal stress at $x_1 = L/2$ when $t = 30$ s.

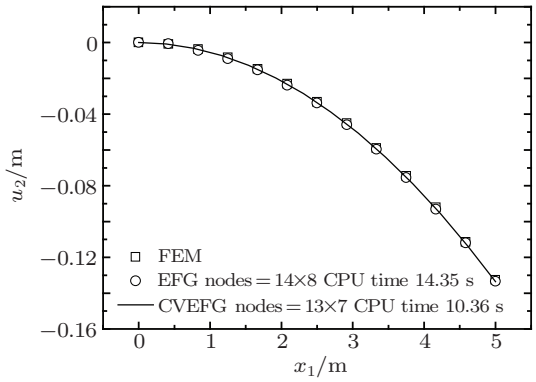


Fig. 12. Vertical displacements of nodes on the neutral axis of the beam when $t = 30$ s.

4.3. Circular ring under a distributed inner pressure

The third example considered is a circular ring under a distributed inner pressure, as shown in Fig. 13. The distributed loading is $p = 30$ kPa. The radii of the circular ring are $a = 2$ m and $b = 5$ m. The volume deformation is elastic, and $E = 1.0 \times 10^6$ Pa, $\nu = 0.25$. The Maxwell model and the Kelvin model are adopted to describe the rheological property of the shear deformation respectively. The parameters in the Maxwell model are $G = 5.0 \times 10^5$ Pa, $\eta = 2.0 \times 10^7$ Pa·s, and the ones in the Kelvin model are $G = 5.0 \times 10^5$ Pa, $\eta = 2.0 \times 10^6$ Pa·s. This example is discussed as a plane strain problem.

The analytical solution of radial displacements in the circular ring obtained using the Maxwell model is given by[31]

$$u_r(r,t) = \frac{pa^2}{b^2 - a^2}\left\{\frac{b^2}{r^2}\left(\frac{1}{G_1} + \frac{1}{\eta}\right) + \frac{r}{2K}\left[1 - \left(\frac{G_1}{6K + G_1}\right)\mathrm{e}^{-\lambda \cdot t}\right]\right\}, \quad (70)$$

where

$$\lambda = \frac{6KG_1}{(6K + G_1)\eta}. \quad (71)$$

Equation (70) is only the solution for a short period of time, and it will be incorrect in the cases of small deformation.

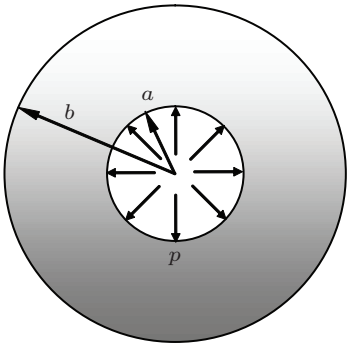


Fig. 13. Circular ring under a distributed inner pressure.

The analytical solution of radial displacements obtained using the Kelvin model is given by[31]

$$u_r(r,t) = \frac{pa^2}{b^2 - a^2}\left[\left(\frac{3r}{6K + G_1}\right)\left(1 - \mathrm{e}^{-\lambda_1 t}\right) + \left(\frac{b^2}{G_1 r}\right)\left(1 - \mathrm{e}^{-G_1 t/\eta}\right)\right], \quad (72)$$

where

$$\lambda_1 = \frac{6K + G_1}{\eta}. \quad (73)$$

Equation (72) shows that the displacement of Kelvin materials equals to 0 at the loading instant. After a long period of time, the displacement will become steady.

By taking advantage of the symmetry of the model, only a quarter of the model needs to be considered in the analysis, as shown in Fig. 14. As given in Fig. 15, 13×15 nodes are used in this example. The scaling parameter $d_{\max}$ is 4.0, and the penalty factor is $\alpha = 1.0 \times 10^2 E$.

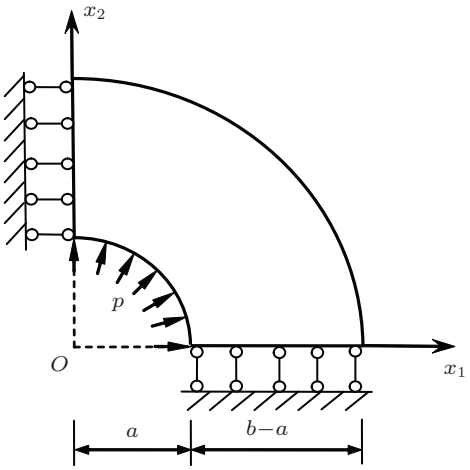


Fig. 14. A quarter of the circular ring with boundary conditions.

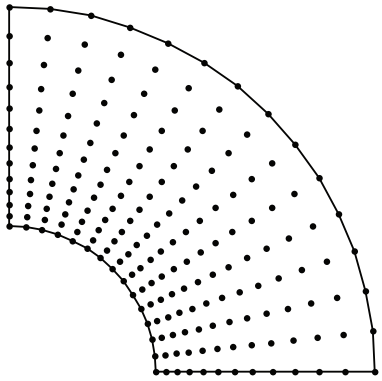


Fig. 15. Node distribution.

The numerical results obtained using the CVEFG and the EFG methods are shown in Figs. 16–19. Form Figs. 16–19, we can see that the results obtained by the CVEFG method are in good agreement with those obtained by the EFG method and the analytical solution.

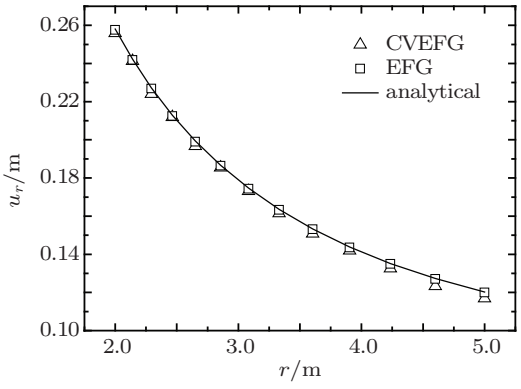


Fig. 16. Radial displacements at $x_2 = 0$ when $t = 30$ s obtained using the Maxwell model.

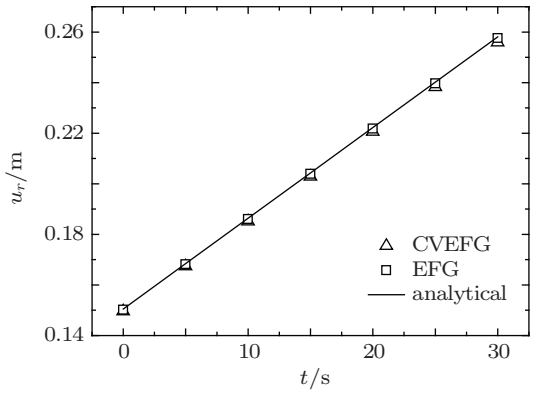


Fig. 17. Time variation of radial displacement at point (2,0) obtained using the Maxwell model.

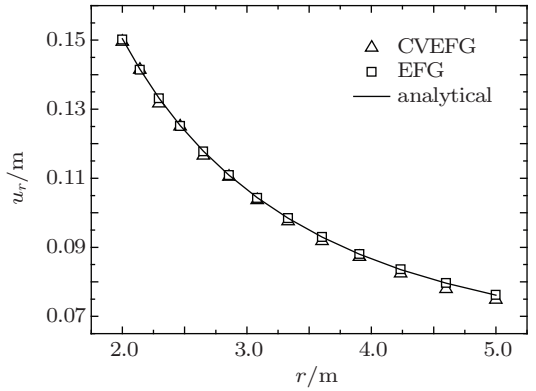


Fig. 18. Radial displacements at $x_2 = 0$ when $t = 30$ s obtained using the Kelvin model.

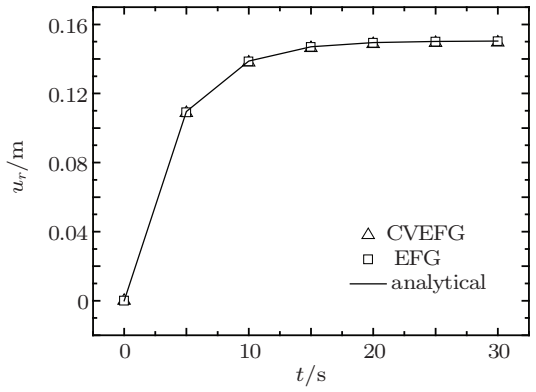


Fig. 19. Time variation of radial displacement at point (2,0) obtained using the Kelvin model.

4.4. Concrete dam under the hydrostatic pressure

To show the validity of the application of the CVEFG method to a complicated engineering problem, a concrete dam under the hydrostatic pressure is considered in this example. The geometric parameters of the dam are shown in Fig. 20. The dam is of 100 m in height, while the upstream water level is 90 m, and

no water exists at the downstream. The bottom of the dam is completely fixed, only the water pressure needs to be considered. The dam is built up with concrete, so the rheological property after completion should be taken into account. The volume deformation of the concrete is elastic, and $E = 2.0 \times 10^{10}$ Pa, $\nu = 0.2$. The three-parameter model is adopted to describe the rheological property of the early-age concrete, and $G_1 = 8.33 \times 10^9$ Pa, $G_2 = 4.0 \times 10^{10}$ Pa, $\eta = 8.0 \times 10^{16}$ Pa·s. This example is discussed as a plane strain problem without considering the gravity.

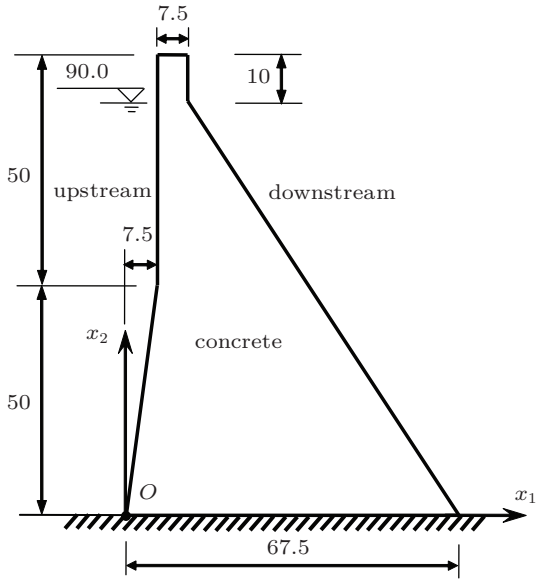


Fig. 20. Schematic diagram of concrete dam under hydrostatic pressure.

As shown in Fig. 21, 255 nodes are used in this example. The scaling parameter $d_{\max}$ is 4.0, and the penalty factor is $\alpha = 1.0 \times 10^2 E$.

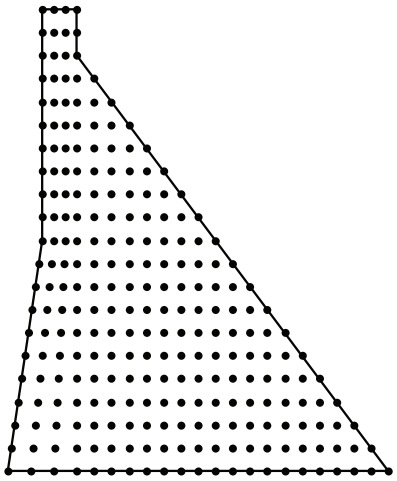


Fig. 21. Node distribution in the dam.

The numerical results obtained by the CVEFG method are shown in Figs. 22 and 23. It is shown that the results obtained using the CVEFG method are in good agreement with those obtained using the EFG method and the FEM. So the validity of the CVEFG method applied to a complicated engineering problem is verified.

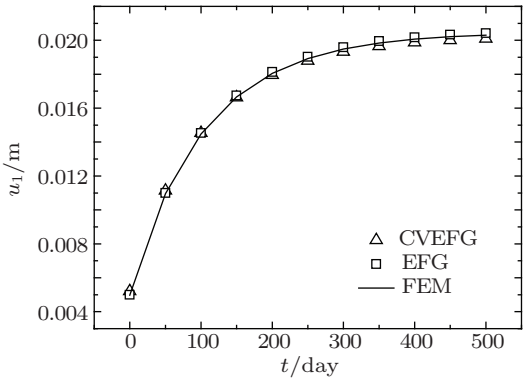


Fig. 22. Time variation of horizontal displacement of the top point (7.5,100).

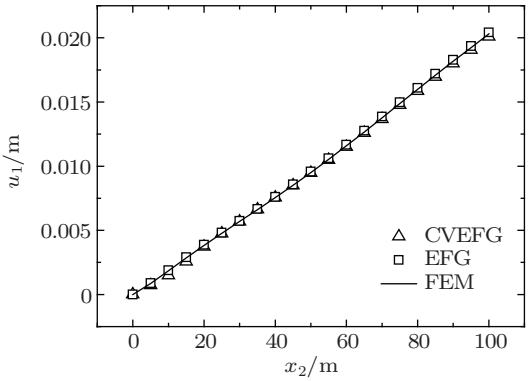


Fig. 23. Horizontal displacements at $x_1 = 15$ when $t = 43200000$ s (500 days).

5. Conclusion

Based on the CVMLS approximation and the EFG method, the CVEFG method for two-dimensional viscoelasticity problems is presented in this paper. The CVEFG method has higher computational precision and efficiency than the EFG method.

Based on the complex variable theory, the CVEFG method in this paper can only solve two-dimensional problems. For three-dimensional problems, we can use the meshless methods based on the IMLS approximation.[32,33] The work in this paper will be a foundation for obtaining the CVEFG methods for elasto-viscoplasticity, viscoelastic large deformation problems and viscoelastic dynamics.

References

[1] Belytschko T, Krongauz Y, Organ D, Fleming M and Krysl P 1996 *Comput. Methods Appl. Mech. Engin.* **139** 3

[2] Cheng Y M and Ji X 1997 *Acta Mech. Solida Sin.* **10** 246

[3] Cheng Y M and Peng M J 2005 *Sci. Chin. Ser.* G: *Phys. Mech. Astron.* **48** 641

[4] Qin Y X and Cheng Y M 2006 *Acta Phys. Sin.* **55** 3215 (in Chinese)

[5] Cheng R J and Cheng Y M 2007 *Acta Phys. Sin.* **56** 5569 (in Chinese)

[6] Dai B D and Cheng Y M 2007 *Acta Phys. Sin.* **56** 597 (in Chinese)

[7] Cheng R J and Cheng Y M 2008 *Acta Phys. Sin.* **57** 6037 (in Chinese)

[8] Cheng R J and Ge H X 2009 *Chin. Phys.* B **18** 4059

[9] Wang J F, Sun F X and Cheng R J 2010 *Chin. Phys.* B **19** 060201

[10] Cheng R J and Ge H X 2010 *Chin. Phys.* B **19** 090201

[11] Wang J F and Cheng Y M 2011 *Chin. Phys.* B **20** 030206

[12] Cheng R J and Cheng Y M 2011 *Chin. Phys.* B **20** 070206

[13] Cheng R J and Cheng Y M 2011 *Acta Phys. Sin.* **60** 070206 (in Chinese)

[14] Lancaster P and Salkauskas K 1981 *Math. Comput.* **37** 141

[15] Cheng Y M and Li J H 2006 *Sci. Chin. Ser.* G: *Phys. Mech. Astron.* **49** 46

[16] Liew K M, Feng C, Cheng Y M and Kitipornchai S 2007 *Int. J. Num. Methods Engin.* **70** 46

[17] Cheng Y M and Li J H 2005 *Acta Phys. Sin.* **54** 4463 (in Chinese)

[18] Cheng Y M, Peng M J and Li J H 2005 *Chin. J. Theor. Appl. Mech.* **37** 719

[19] Liew K M and Cheng Y M 2009 *Comput. Methods Appl. Mech. Engin.* **198** 3925

[20] Chen L and Cheng Y M 2010 *Sci. Chin. Ser.* G: *Phys. Mech. Astron.* **40** 242 (in Chinese)

[21] Chen L and Cheng Y M 2010 *Chin. Phys.* B **19** 090204

[22] Peng M J, Liu P and Cheng Y M 2009 *Int. J. Appl. Mech.* **1** 367

[23] Peng M J, Li D M and Cheng Y M 2011 *Engin. Struct.* **33** 127

[24] Li D M, Peng M J and Cheng Y M 2011 *Sci. Chin. Ser.* G: *Phys. Mech. Astron.* **41** 1003 (in Chinese)

[25] Bai F N, Li D M, Wang J F and Cheng Y M 2012 *Chin. Phys.* B **21** 020204

[26] Yang H T and Liu Y 2003 *Int. J. Solids Struct.* **40** 701

[27] Sladek J, Sladek V and Zhang C 2005 *Engin. Anal. Bound. Elem.* **29** 597

[28] Sladek J, Sladek V, Zhang C and Schanz M 2006 *Comput. Mech.* **37** 279

[29] Guan Y J, Zhao G Q, Wu X and Lu P 2007 *J. Mater. Process Tech.* **187** 412

[30] Canelas A and Sensale B 2010 *Engin. Anal. Bound. Elem.* **34** 845

[31] Flügge W 1975 *Viscoelasticity* (2nd edn.) (New York: Springer-Verlag) p. 1

[32] Zhang Z, Liew K M and Cheng Y M 2008 *Engin. Anal. Bound. Elem.* **32** 100

[33] Zhang Z, Liew K M, Cheng Y M and Lee Y Y 2008 *Engin. Anal. Bound. Elem.* **32** 241